Tuning of *g*-factor in self-assembled In(Ga)As quantum dots through strain engineering

T. Nakaoka,[1] T. Saito,[2] J. Tatebayashi,[1] S. Hirose,[3] T. Usuki,[3] N. Yokoyama,[3] and Y. Arakawa[1]
[1]*Research Center for Advanced Science and Technology, University of Tokyo, 4-6-1 Komaba, Meguro-ku, Tokyo 153-8904, Japan*
[2]*Center for Collaborative Research, University of Tokyo, 4-6-1 Komaba, Meguro-ku, Tokyo 153-8904, Japan*
[3]*Fujitsu Laboratories Ltd., 10-1 Morinosato-Wakamiya, Atsugi 243-01, Japan*
(Received 27 January 2005; published 2 May 2005)

We have investigated the effect of strain on the *g*-factors of self-assembled In(Ga)As dots by single-dot spectroscopy and an eight-band effective mass calculation taking into account the influence of the strain distribution and the Zeeman effect. The strain and its distribution in and around the quantum dots are varied by thermal annealing or by introducing an strain reducing layer. Thermal annealing produces a graded composition profile due to In—Ga intermixing. The graded composition profile reduces both hydrostatic and biaxial strain near the bottom of the dot, and enhances them near the top. This strain variation results in a large reduction of the absolute hole *g*-value and a small reduction of the absolute electron *g*-value. On the other hand, the covering of InAs dots with an $In_{0.17}Ga_{0.83}As$ strain reducing layer decreases mainly the hydrostatic strain. The variation of the strain and the band edge alignment enhance the electron *g*-value while they reduce the hole *g*-value. These results should provide insights to control the *g*-factors in pyramidal self-assembled dots.

DOI: 10.1103/PhysRevB.71.205301 PACS number(s): 78.67.Hc, 75.75.+a, 73.22.−f, 78.55.−m

I. INTRODUCTION

The possibility of using the spin degree-of-freedom of electrons for encoding quantum information has recently attracted significant attention. Knowledge of electron and hole *g*-factors, which are the coefficient connecting spin moment with magnetic one, is important to design such spin-based devices. For example, the system with a large *g*-factor is preferable for controlling spin-qubit while near-zero electron *g*-factor is suitable to design a quantum receiver.[1,2] In addition, coherent spin manipulation which is an important requirement for the quantum information processing has been demonstrated by modulating *g*-factor anisotropy.[3,4]

One of the promising candidates for the basic units of quantum information processing in solid state systems is self-assembled quantum dots. The strong three-dimensional confinement of carriers[5] provides the ability to control the number of electrons,[6,7] long spin lifetime and expected long decoherence time.[8–11] The *g*-factors of self-assembled dots have been evaluated by optical measurements[12–16] and transport measurements.[17–19] The measured values of the *g*-factors are quite different from bulk ones[20] due to size quantization,[21–23] and probably their peculiar structural properties such as composition and strain distributions although their effects and the way to modify the *g*-factor have not been well understood.

One way to modify the structural and electronic properties of quantum dots is thermal annealing. Thermal annealing has been widely used to tune their emission energies, the inhomogeneous broadening,[24,25] the fine-structure splitting,[26,27] and the exciton dephasing time.[28] A significant narrowing and blueshift of the emission have been attributed to strong In—Ga intermixing and the following variation of strain distribution. The composition and strain distribution strongly affect the electronic properties of self-assembled dots.[29,30] Although magneto-optical properties of the annealed quantum dots have been also intensively studied,[16,31] the roles of composition and strain distribution have not been clear. Another way to modify the structural and electronic properties of quantum dots is to cover the dots with a strain reducing layer (SRL). The covering and embedding of the InAs dots with SRL have been widely used to decrease the emission energy to achieve telecommunication wavelengths.[32–36] The decreased emission energy has been mainly attributed to decreased hydrostatic strain.

In this paper, *g*-factor variations due to thermal annealing or introduction of SRL in InGaAs and InAs quantum dots have been measured by single dot spectroscopy and modelled by the eight-band $\mathbf{k}\cdot\mathbf{p}$ theory using a realistic three-dimensional picture. The single dot measurement permits a separation of the emission lines of single electron-hole pairs from those of multiparticle states. The separation allows comparison of the experiment with the eight-band effective mass calculation of single particle bound-states avoiding the multiparticle effects of carriers. We obtain good agreement between the result of single dot spectroscopy and that of the calculation. These investigations show that the *g*-factor modification observed experimentally is not reproduced by simply weighing the material dependent bulk values with the charge density, but is caused mainly by strain-induced modification of the confining potential. The calculation shows how strain modifies electron and hole *g*-factors. The results will serve to find an appropriate way to tune electron and hole *g*-factors. The outline of this paper is the following: In Sec. II and Sec. III, we will present our experimental and calculation procedures, respectively; Sec. IV A gives the experimental and calculated results on thermally annealed dots. We will show that the experimentally measured *g*-factors of the annealed dots agree with the calculated one assuming nonuniform graded composition profiles while the experimental *g*-factors of as-grown dots agree with the calculated ones assuming uniform composition profiles. We will discuss the effect strain profile altered by the nonuniform graded composition. Section IV B provides the effect of an

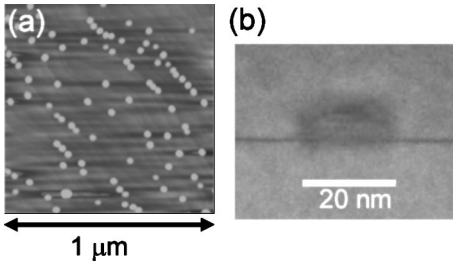

FIG. 1. (a) AFM image of uncapped InAs quantum dots. (b) TEM image of InAs quantum dots embedded in a GaAs barrier.

$In_{0.17}Ga_{0.83}As$ strain reducing layer on the *g*-factor of self-assembled InAs quantum dots. We will show that the introduction of SRL modifies not only the emission energy, but also the electron and the hole *g*-factors. In Sec. V we finally summarize our findings.

II. EXPERIMENT

Self-assembled quantum dots used in this work were grown on a GaAs (100) wafer at 500 °C and 76 Torr by metal organic chemical vapor deposition. We studied the self-assembled dots grown with nominal composition of InAs and $In_{0.5}Ga_{0.5}As$, which are called "InAs" dots and "InGaAs" dots, respectively, in this paper. We studied four samples, two of which are as-grown InGaAs and InAs quantum dots. The third was annealed InGaAs dots which are annealed at 700 °C for 1 h after the growth. In these three samples, the dots were covered with a 100 nm GaAs layer. Finally, we also studied the InAs dots covered with a 5-nm-thick $In_{0.17}Ga_{0.83}As$ SRL layer followed by a 100 nm GaAs layer. Figure 1(a) shows atomic force microscopy (AFM) image of reference uncapped InAs quantum dots. The measurement revealed the average dot diameter of 20 nm with a standard deviation of 3 nm and the height of 7 nm with a standard deviation of 2 nm, as well as the areal density of $1.3\times10^{10}/cm^2$ for both the InAs and the InGaAs dots. Very similar diameter and height of GaAs-capped InAs dots to those of uncapped ones were revealed by cross-sectional transmission electron microscopy (TEM), as shown in Fig. 1(b).

Magnetophotoluminescence spectroscopy was performed in Faraday configuration at 3.5 K on small mesa structures with lateral dimensions of 200 nm. The photoluminescence was excited with the 632.8 nm line of a He—Ne laser beam focused by a microscope objective to a diameter of about 2 μm. The excitation power was limited to 10 W/cm^2. The photoluminescence from a mesa structure was collected by the objective, dispersed by a double grating monochromator, and detected by a Si CCD or an InGaAs detector array. By using these two detectors we could study the *g*-factors in almost the whole emission energy range of the four types of quantum dots.

III. THEORY

Our calculation method is based on an eight-band effective mass model which includes the conduction, heavy, light, and split-off carriers for a total of eight bands.[37–39] In the absence of magnetic fields, the eight-band model has been successfully applied for pyramidal quantum dots.[40–42] We have computed the energies and wave functions by the finite difference method where the material parameters and strain are varied from site to site. Our model includes the effects of strain piezoelectricity, valence band (VB) mixing, the interaction between the conduction band (CB) and the VB, and the Zeeman effect. The effective mass Hamiltonian in bulk materials is given in Ref. 38. In the presence of a magnetic field, the wave vector $\mathbf{k}$ in the effective mass Hamiltonian is replaced by the operator $\mathbf{k}=-i\nabla+e/\hbar\mathbf{A}$, where $\mathbf{A}$ is the vector potential.

The quantum dots are modelled by a pyramidal shape with a diagonal length of 21.2 nm and a height of 7.5 nm to compare the measured dots with a diameter of 20 nm and a height of 7 nm on average, revealed by AFM and TEM measurement. We note that the dot size is fixed for the calculation in this paper to focus on the effect of strain. As we shall show below, the essential feature of the *g*-factor variation is reproduced by the calculation assuming the fixed dot size. Relatively high size-uniformity of our dots and small size-variation following the annealing and the capping with SRL are supported by the similar distribution of the diamagnetic coefficients in the quantum dots. The diamagnetic coefficients of all the measured dots range from 7 to 11 $\mu eV/T^2$. No systematic difference is found among the diamagnetic coefficients of the as-grown GaAs-capped dots, the annealed dots, and the SRL-capped dots in contrast to the apparent difference found in their *g*-factors. In the calculation, wetting layer is omitted to avoid exorbitant computational expense and to focus on the strain variation following annealing or SRL-capping. The wetting layer may be treated separately as a slight increase of the dot height because it does not significantly modify the characteristics of the strain distribution in the dots.[43] The strain in the modelled structure is calculated by a three-dimensional finite element analysis. To reproduce the measured dots in the small mesa structure, a free boundary condition is applied at the surface of a cube in which the pyramidal quantum dot is embedded. We have solved the Schrödinger equation for the multicomponent spinor of the envelope functions. The details of the Hamiltonian, the base functions, and the material parameters used in the calculation are described in Ref. 44.

IV. RESULTS AND DISCUSSION

A. Thermally annealed quantum dots

Typical magnetic field dependence of the photoluminescence spectrum from a single annealed InGaAs dot is shown in Fig. 2(a). The emission lines have a linewidth of about 50 μeV. With increasing magnetic field (B), the unpolarized emission line splits into an oppositely circularly polarized doublet. The energy shift of the center of the doublet, which represents a diamagnetic shift, is quadratic in B with a constant of 9.37 $\mu eV/T^2$ [Fig. 2(b)]. The splitting magnitude increases linearly with B [Fig. 2(c)]. By fitting the data in Fig. 2(c), we obtain the exciton *g*-factor $g_{ex}=-1.83$, which is defined in this paper as $g_{ex}=\{E(\sigma^+)-E(\sigma^-)\}/(\mu_B B)$, where

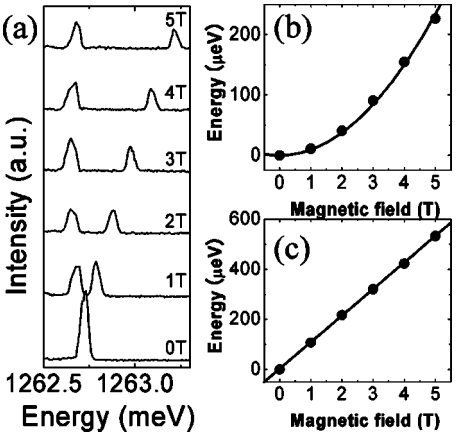

FIG. 2. (a) Photoluminescence spectra of the annealed InGaAs dots for magnetic fields indicated. All the spectra are obtained without polarization selectivity. (b) The center position of the doublet in (a) as a function of magnetic field. The solid curve is a quadratic fit. (c) The splitting magnitude of the doublet in (a). The solid line is a linear fit.

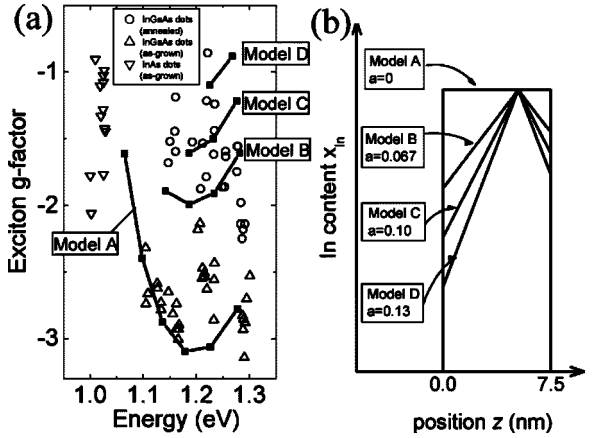

FIG. 3. Exciton g-factors plotted as a function of the ground state emission energy. Open symbols shows the experimentally obtained g-factors of the InAs dots, the InGaAs dots and the annealed dots. Solid squares, connected by lines to guide the eyes, give the exciton g-factors calculated for the models shown in (b). The composition of the dots are represented by the emission energy. (b) Schematic representation of the four structural models used in this work. In Model A, the dots have a uniform In composition. In Models B, C, and D, the dots have nonuniform In compositions. The In composition x_{In} is represented as $x_{\mathrm{In}}=\pm a(z-0.7H)+x_{\max}$, where H is the dot height ($H=7.5$ nm), z is the position along the growth direction. The solid squares in (a) correspond to $x_{\max}=1$, 0.9, 0.8, 0.7, 0.6, and 0.5 in Model A, $x_{\max}=1$, 0.9, 0.8, and 0.7 in Model B, $x_{\max}=1$, 0.9, and 0.8 in Model C, $x_{\max}=1$ and 0.9 in Model D.

$E(\sigma^+)$ and $E(\sigma^-)$ are the energies of σ^+ and σ^- polarized emissions, respectively. Such quadratic diamagnetic shift and linear Zeeman splitting suggests a high symmetry of our dots.[44,45] The magnetic field dependence is very similar to those of the as-grown InGaAs and InAs dots except for the splitting magnitude. The experimentally obtained exciton g-factors of 25 annealed InGaAs dots are plotted in Fig. 3(a) in addition to the g-factors of 30 as-grown InGaAs dots and 10 as-grown InAs dots measured in a previous work.[44] The experimental errors are less than the size of the symbols in the figure. The scatter beyond the errors represents the inhomogeneity of the quantum dots. We find that the absolute value of the exciton g-factor $|g_{\mathrm{ex}}|$ of the InGaAs dots are reduced by the thermal annealing. The exciton g-factor of the annealed InGaAs dots ranges from -2 to -1 while that of as-grown one ranges from -3 to -2.

The effect of thermally induced intermixing is calculated by taking into account nonuniform composition profiles. Both In-diluting and In-enriching compositional changes mainly along the growth direction have been reported.[46,47] To reproduce a higher average In content near the top of the dots than the bottom as well as vertical In-interdiffusion out of the dots, we use the models B–D with peaked In composition gradient, as shown in Fig. 3(b). We focus on the ground states of the lowest conduction band (CB) and the highest valence band (VB). The calculation shows that the twofold degenerate (Kramers's degeneracy) states of the CB and VB split into doublets in presence of a magnetic field, due to the Zeeman effect. From the splitting we obtain the CB g-factor $g_c \equiv \{E(c^+)-E(c^-)\}/(\mu_B B)$, and the VB g-factor $g_v \equiv \{E(hh^+)-E(hh^-)\}/(\mu_B B)$, where the signs $(\pm)$ on the top label the sign of the z-component of the total angular momentum. Using the optical selection rule, we obtain the energies of σ^+ and σ^- polarized emissions neglecting e-h Coulomb interaction which does not play significant role in this weak magnetic field range. The calculation reproduces the experimental magnetic field dependence such as a nearly quadratic diamagnetic shift with a coefficient of about 10 μeV/T^2 and a linear Zeeman splitting. From the splitting magnitude, we obtain the exciton g-factor $g_{\mathrm{ex}}=-g_c+g_v$.

Figure 3(a) compares the experimental exciton g-factors of thermally annealed dots and the calculated ones for the dots with various composition and its gradients represented by Models A, B, C, and D. The exciton g-factors are plotted as a function of the ground-state transition energy. Most of the experimental exciton g-factors of the as-grown InAs and In-GaAs dots agree with those calculated for Model A with uniform composition profiles. Not only the quantitative values of the exciton g-factors, but also smaller $|g_{\mathrm{ex}}|$ of the InAs dots than that of the InGaAs dots is well reproduced. Such a characteristic composition dependence is mainly due to stronger off-diagonal $\mathbf{k}\cdot\mathbf{p}$ coupling between the valence bands in the InAs dots than that in the InGaAs dots.[44] On the other hand, the g-factors of the annealed InGaAs dots agree with those calculated for Models B, C, and D with nonuniform composition profiles. It is important to note that within the uniform composition model (Model A) any composition variation cannot reproduce the experimental g-factor of the annealed dots.[48] The variation of the g-factors due to the thermal annealing can be explained by using the graded composition profiles as represented by Models B, C, and D. The experimental g-factor distribution ranging from Model B to D may reflect different degree of intermixing from dot to dot.

In the following, we discuss the cause of the small $|g_{\mathrm{ex}}|$ in the dots with graded compositions. Figure 4 plots the CB g-factor and the VB g-factor separately. Both the absolute values of the CB g-factor $|g_c|$ and the VB g-factor $|g_v|$ are

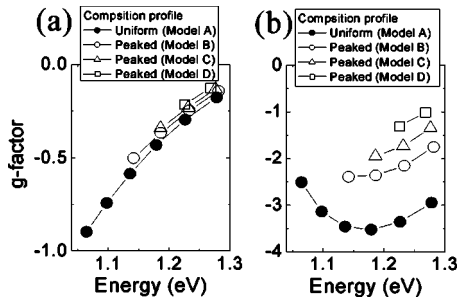

FIG. 4. (a) CB g-factor and (b) VB g-factor calculated for the dots with various composition and profile (see the caption of Fig. 3), plotted as a function of the ground transition energy. The lines are to guide the eye.

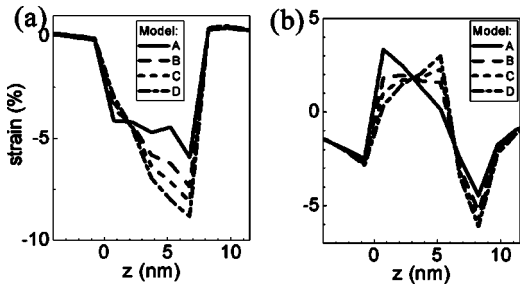

FIG. 5. (a) Hydrostatic and (b) biaxial strain distributions in and around the quantum dots with various composition gradients represented in Model A, B, C, and D. The composition averaged for the whole dot volume is fixed to 0.5.

decreased as the composition is graded at a fixed emission energy. There is a tendency that the CB g-factor strongly depends on the emission energy while the VB g-factor rather depends on the composition profile. The CB g-factor seems modified following the variation of the VB g-factor in addition to the principal variation determined by the emission energy. In other words, smaller $|g_c|$ corresponds to smaller $|g_v|$ at a fixed emission energy. This tendency is also seen in the size and shape dependence of the pyramidal InGaAs dots.[44] In the following discussion, to extract the effect of the composition and strain profile on the g-factors, we vary the composition gradients under the condition that the composition averaged over the whole dot volume is fixed. The condition keeps the emission energy nearly constant. For example, when the composition gradient a is varied from 0 to 0.13 in the dots with the average composition of 0.5, $|g_c|$ and $|g_v|$ are reduced by 20% and 60%, respectively, although other electronic properties such as the emission energy and the wave function spill over are nearly unchanged. The emission energy ranges from 1.26 eV to 1.28 eV in the dots. The composition gradient variation increases the electron and the hole charge densities in the dots only by 4.4% and 0.78%, respectively. The estimated variations are too small to explain the reduction of $|g_c|$ and $|g_v|$, caused by grading the composition. It should be noted that the large g-factor variation cannot be explained by the composition-dependent bulk g-values which differ from site to site according to the graded composition profile. The effect of the composition-dependent bulk g-values is estimated by weighing the bulk values with the charge density distributed in and around the dot. The $|g_c|$ and $|g_v|$ are estimated to be increased by 27% and 19%, respectively, as the composition gradient a is varied from 0 to 0.13 at the fixed average composition 0.5. This reflects the increase of the local In composition at the sites where the charges are localized. The variation differs from that obtained by the $\mathbf{k}\cdot\mathbf{p}$ calculation even qualitatively.

The large reduction of the g-values despite the increase of the effective In composition is attributed to the shape change of the wave function, or the change of its component. They are induced by the variation of the confining potential determined by the strain distribution in addition to the band edge alignment without the strain effects. The strain distributions in the dots with different composition gradients are shown in Fig. 5. As the composition is graded from $a=0$ to 0.13, both hydrostatic and biaxial strains near the bottom of the dots are reduced due to the decreased composition difference from the GaAs barrier while the strains near the top are enhanced reflecting the increase of the composition difference. The strain variation modifies the confining potentials to vary the electron and hole wave functions along the growth direction.

In particular, the modification of the hole confining potential is important because in pyramidal InGaAs dots the VB g-factor strongly depends on the dot size and shape or the confining potential. The hole confining potential is varied largely by the biaxial strain distribution besides the hydrostatic one. The strain variation modifies the hole confining potential to delocalize the hole along the growth direction. In other words, the heavy-hole character of the hole wave function is reduced. Because the heavy-hole g-value is larger than the light-hole and split-off g-values in the bulk semiconductor in the Faraday configuration, the reduction of the heavy-hole character decreases $|g_v|$. Thus, the VB g-factor is modified by the annealing. The variation of the VB g-factor affects the CB g-factor due to CB-VB $\mathbf{k}\cdot\mathbf{p}$ coupling. The decrease of $|g_c|$ with grading the composition at a fixed ground transition energy is accompanied by the decrease of $|g_v|$ caused by the variation of the shape of the confining potential. The composition grating results in the decrease of $|g_{ex}|$ because the CB g-factor value is much smaller than the VB g-factor value in all the calculated dots.

B. InAs quantum dots with SRL

Now we study the strain variation by introducing the 5-nm-thick $In_{0.7}Ga_{0.83}As$ SRL layer and the effect on the g-factor. Typical magnetic field dependence of the photoluminescence emission from a single InAs dot covered with the SRL is shown in Fig. 6(a). The emission lines have a linewidth of about 70 μeV, which is close to those of the dots without the SRL, ranging from 40 μeV to 90 μeV. This narrow linewidth suggests that the SRL can modify the electronic states, keeping the long decoherence time of the self-assembled dots. With increasing magnetic field (B), the unpolarized emission line splits into an oppositely circularly polarized doublet. The diamagnetic shift of the center of the doublet is quadratic in B with a constant of 9.5 $\mu eV/T^2$ [Fig. 6(b)]. The splitting magnitude increases linearly with B [Fig. 6(c)]. The exciton g-factor is $g_{ex}=-0.45$. Such quadratic dia-

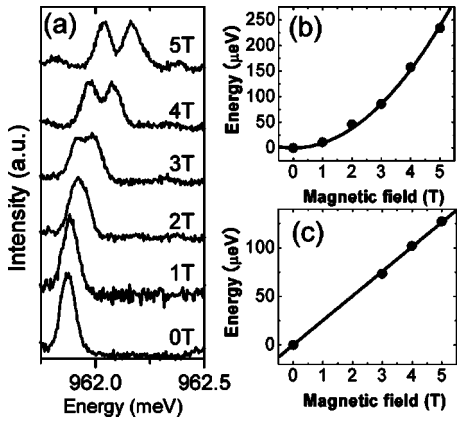

FIG. 6. (a) Single dot photoluminescence spectrum for the InAs dots covered with $In_{0.17}Ga_{0.83}As$ layer for magnetic fields indicated. All the spectra are obtained without polarization selectivity. (b) The center position of the doublet in (a) as a function of magnetic field. The solid curve is a quadratic fit. (c) The splitting magnitude of the doublet well resolved above 3 T, as shown in (a). The solid line is a linear fit.

magnetic shift and linear Zeeman splitting are very similar to those of the dots without the SRL except for the splitting magnitude, or the g-factor value. The experimental exciton g-factors of 20 InAs dots with the SRL and those of 16 dots without the SRL are plotted as a function of the emission energy in Fig. 7(a). The absolute value of the exciton g-factor $|g_{ex}|$ of the dots with the SRL is smaller than that of the dots without the SRL. The exciton g-factor of the dots with the SRL ranges from −1 to 0 while that without the SRL ranges from −2 to −1.

We investigate here the SRL effect on the g-factor theoretically. We apply Model A with an uniform composition profile to reproduce the nonannealed dots. The modelded quantum dot is covered with an $In_{0.17}Ga_{0.83}As$ layer. The calculated exciton g-factors are plotted in Fig. 7(b) as a function of the ground-state transition energy. The redshift of the emission energy and the reduction of $|g_{ex}|$ with introducing the SRL are reproduced. The slight disagreement in the emission energy may be improved by finely tuning the dot-shape.[46] Although the experimental exciton g-value of

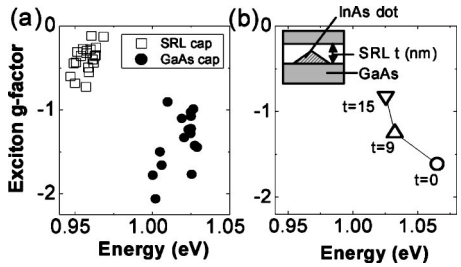

FIG. 7. (a) Experimentally evaluated exciton g-factors of the InAs dots capped with $In_{0.17}Ga_{0.83}As$ SRL and those of the dots capped with GaAs, plotted as a function of the ground state emission energy. (b) Calculated exciton g-factors of the InAs dot capped with 0 nm-SRL (without SRL), 9 nm-SRL or 15 nm-SRL. Schematic sample structure is shown in the inset. Symbols are connected by lines to guide the eyes.

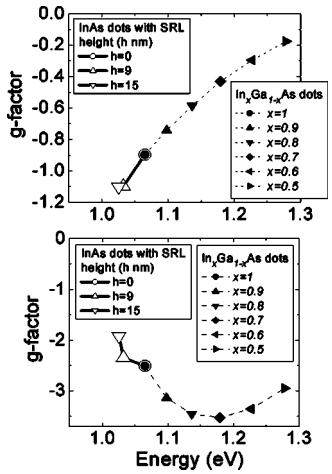

FIG. 8. (a) CB g-factor and (b) VB g-factor calculated for various dots with the same size and shape. Closed symbols connected by dotted lines to guide the eyes represent the g-factors of the $In_xGa_{1-x}As$ dots, which are the same ones shown in Fig. 2 (Model A). Open symbols connected by solid lines represent the g-factors of the InAs dots with different SRL thickness.

the InAs dots without the SRL is quantitatively reproduced by the calculation, the experimental g-value of the dots with the SRL is reproduced by the calculation for the modelled dots with a much thicker SRL than the experiment. This may be due to the nonflat surface of the experimental SRL induced by the SRL-growth directly onto the quantum dot. In addition, slight interdiffusion among InAs dots, $In_{0.17}Ga_{0.83}As$ layer, and GaAs barrier may take place because the $In_{0.17}Ga_{0.83}As$ layer was grown at much slower rate than GaAs. In our simple model with the flat uniform SRL as shown in the inset of Fig. 7(b), the influence of the nonflat SRL and interdiffused environment may be represented by using the SRL thicker than the dot height.

In the following, we discuss the cause of the small $|g_{ex}|$ in the dots with the SRL on the basis of the $\mathbf{k}\cdot\mathbf{p}$ calculation which has reproduced the essential effect of the SRL at least qualitatively. Figure 8 plots the calculated CB g-factor and the VB g-factor separately. The absolute CB g-value $|g_c|$ increases with increasing the SRL thickness while the absolute VB g-value $|g_v|$ decreases. Consequently the exciton g-factor represented as $|g_{ex}|=-|g_c|+|g_v|$ in our calculated dots decreases. The increase of $|g_c|$ has been observed also by capacitance spectroscopy for an ensemble of InAs dots.[19] As in that paper, g-factor variation is widely explained by weighing the material dependent bulk g-factors with the corresponding charge density distributed in the dot and the barrier regions. However, the g-factor variation estimated by weighing the bulk g-values of InAs, $In_{0.17}Ga_{0.83}As$ (SRL), and GaAs, with the charge densities in the dot and the barriers differs from that measured experimentally, and that calculated by the $\mathbf{k}\cdot\mathbf{p}$ model even qualitatively. As the SRL thickness is increased from 0 nm to 15 nm, the electron charge density in the dot decreases from 87% to 84%, and the hole charge density decreases from 93% to 89%. The decreased charge density in the dot with larger g-values than the barriers decreases $|g_c|$ and $|g_v|$ by 1.0% and 2.0%, respectively. The variation contradicts an increase of $|g_c|$ by 23% and a

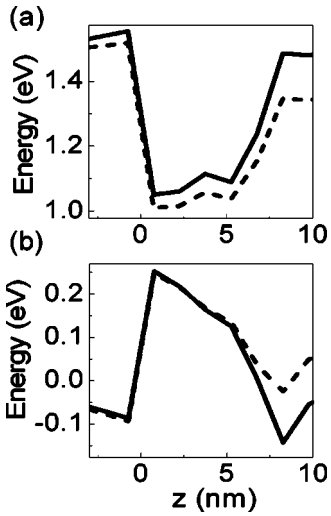

FIG. 9. (a) Energy of the CB edge and (b) the VB edge in and around an InAs dot without SRL (solid lines) or with 15 nm SRL (dotted lines), plotted along the growth direction z through the center of the dot.

decrease of $|g_v|$ by 24%, calculated by the $\mathbf{k}\cdot\mathbf{p}$ model.

To discuss other causes to vary the g-factor, we show in Fig. 8 the composition dependence of the g-factors of $In_xGa_{1-x}As$ dots without the SRL as well as those of the SRL-capped InAs dots. The CB g-factors of the InAs dots with SRL almost agree with the extrapolation of the composition dependence to low emission energy while the VB g-factor deviates from the extrapolation. This feature is consistent with the size and the shape dependence of the g-factors calculated by the $\mathbf{k}\cdot\mathbf{p}$ theory.[44] The calculation has shown that the CB g-factor strongly depends on the emission energy rather than the size and the shape in pyramidal $In_xGa_{1-x}As$ dots while the VB g-factor rather depends on the size and the shape of the dot, or the confining potential, in addition to the emission energy. Capping the dot with SRL should give similar effect because it modifies the strain in and around the dot, and consequently the confining potential.

The strain induced modifications of the CB and the VB edges are shown in Fig. 9. By capping the dot with the SRL, the CB edge of the InAs dot is lowered due to the relaxation of the hydrostatic strain in the dot region while the VB edge around the bottom of the dot is nearly unchanged due to the small hydrostatic deformation potential and the compensation between the effects of the hydrostatic strain and the biaxial strain. The variations of the CB and VB edges largely decreases the emission energy, or the energy difference between the ground CB state and the VB state, which results in the enhancement of $|g_c|$. While the VB edge near the bottom is nearly unchanged, the VB edge near the top of the dot is raised due to the relaxation of the biaxial strain and the reduction of the band offset between the dot and the capping material. Such a variation of the VB edge corresponds to a height increase of the dot, and delocalizes the hole along the growth direction. In other words, the variation decreases the heavy-hole character of the hole wave-function. Thus, the VB edge variation reduces $|g_v|$.

V. SUMMARY

In summary, the exciton g-factors of the as-grown dots capped by GaAs, the annealed quantum dots, and dots capped by $In_{0.17}Ga_{0.83}As$ are measured by single-dot spectroscopy. The g-factors are reproduced by the calculation based on the eight-band $\mathbf{k}\cdot\mathbf{p}$ model. We have shown that thermal annealing reduces both CB g-value and VB g-value while SRL-capping enhances the CB g-value and reduces the VB g-value. The g-factor variation due to the thermal annealing is reproduced by the variation of the composition profile from uniform to graded one. The variation of the biaxial strain is important for the g-factor variation. The strain relaxation near the bottom of the dot delocalizes the hole along the growth direction. The decrease of the heavy-hole character decreases $|g_v|$, and also decreases $|g_c|$ through the CB-VB $\mathbf{k}\cdot\mathbf{p}$ coupling. In the dots capped by $In_{0.17}Ga_{0.83}As$ SRL, the enhancement of $|g_c|$ is attributed to the largely decreased hydrostatic strain while the reduction of $|g_v|$ is attributed to the decreased heavy-hole character induced by strain and band-offset variation. Thus, the results give an understanding of the effect of the strain on the g-factor, and should open the way to engineer the g-factors. In particular, the way to enhance $|g_c|$ is important for spin-based applications. By using the SRL, $|g_c|$ is increased beyond the composition dependence. In addition, we have shown that the capping with the SRL extends the emission wavelength to approximately 1.3 μm, almost keeping the narrow homogenous linewidth corresponding to the decoherence time. The controllability of the g-factors of the dots emitting in telecommunication wavelengths should be useful in the applications to the quantum information devices using single electron spin and single photon, such as single photonemitters,[49] single photoelectron transistors[2] that convert a photon polarization to an electron-spin polarization, and a basic unit of quantum information processing.[9]

ACKNOWLEDGMENTS

We thank T. Kakitsuka for assistance in the calculations. This work was supported in part by the Focused Research and Development Project for the Realization of the World's Most Advanced IT Nation, IT Program, MEXT.

[1] R. Vrijen and E. Yablonovitch, Physica E (Amsterdam) **10**, 569 (2001).

[2] H. Kosaka, D. S. Rao, H. D. Robinson, P. Bandaru, K. Makita, and E. Yablonovitch, Phys. Rev. B **67**, 045104 (2003).

[3] Y. Kato, R. C. Myers, A. C. Gossard, and D. D. Awschalom, Nature (London) **427**, 50 (2004).

[4] Y. Kato, R. C. Myers, D. C. Driscoll, A. C. Gossard, J. Levy, and D. D. Awschalom, Science **299**, 1201 (2003).

[5] Y. Arakawa and H. Sakaki, Appl. Phys. Lett. **40**, 939 (1982).
[6] T. Sato, T. Yamaguchi, W. Izumida, S. Tarucha, H. Z. Song, T. Miyazawa, Y. Nakata, T. Ohshima, and N. Yokoyama, Physica E (Amsterdam) **21**, 506 (2004).
[7] T. Ota, K. Ono, M. Stopa, T. Hatano, S. Tarucha, H. Z. Song, Y. Nakata, T. Miyazawa, T. Ohshima, and N. Yokoyama, Phys. Rev. Lett. **93**, 066801 (2004).
[8] A. I. Tartakovskii, J. Cahill, M. N. Makhonin, D. M. Whittaker, J-P. R. Wells, A. M. Fox, D. J. Mowbray, M. S. Skolnick, K. M. Groom, M. J. Steer, and M. Hopkinson, Phys. Rev. Lett. **93**, 057401 (2004).
[9] A. Imamoglu, D. D. Awschalom, G. Burkard, D. P. DiVincenzo, D. Loss, M. Sherwin, and A. Small, Phys. Rev. Lett. **83**, 4204 (1999).
[10] S. Cortez, O. Krebs, S. Laurent, M. Senes, X. Marie, P. Voisin, R. Ferreira, G. Bastard, J.-M. Gerard, and T. Amand, Phys. Rev. Lett. **89**, 207401 (2002).
[11] M. Kroutvar, Y. Ducommun, D. Heiss, M. Bichler, D. Schuh, G. Abstreiter, and J. Finley, Nature (London) **432**, 81 (2004).
[12] Y. Toda, S. Shinomori, K. Suzuki, and Y. Arakawa, Appl. Phys. Lett. **73**, 517 (1998).
[13] M. Bayer, A. Kuther, A. Forchel, A. Gorbunov, V. B. Timofeev, F. Schäfer, J. P. Reithmaier, T. L. Reinecke, and S. N. Walck, Phys. Rev. Lett. **82**, 1748 (1999).
[14] M. Bayer, G. Ortner, O. Stern, A. Kuther, A. A. Gorbunov, A. Forchel, P. Hawrylak, S. Fafard, K. Hinzer, T. L. Reinecke, S. N. Walck, J. P. Reithmaier, F. Klopf, and F. Schäfer, Phys. Rev. B **65**, 195315 (2002).
[15] J. J. Finley, D. J. Mowbray, M. S. Skolnick, A. D. Ashmore, C. Baker, A. F. G. Monte, and M. Hopkinson, Phys. Rev. B **66**, 153316 (2002).
[16] A. R. Goñi, H. Born, R. Heitz, A. Hoffmann, C. Thomsen, F. Heinrichsdorff, and D. Bimberg, Jpn. J. Appl. Phys., Part 1 **39**, 3907 (2000).
[17] A. S. G. Thornton, T. Ihn, P. C. Main, L. Eaves, and M. Henini, Appl. Phys. Lett. **73**, 354 (1998).
[18] M. C. Bodefeld, R. J. Warburton, K. Karrai, and J. P. Kotthaus, G. Medeiros-Ribeiro, and P. M. Petroff, Appl. Phys. Lett. **74**, 1839 (1999).
[19] G. Medeiros-Ribeiro, E. Ribeiro, and H. Westfahl Jr., Appl. Phys. A: Mater. Sci. Process. **77**, 725 (2003).
[20] H. Kosaka, A. A. Kiselev, F. A. Baron, K-W. Kim, and E. Yablonovitch, Electron. Lett. **37**, 464 (2001).
[21] A. A. Kiselev, E. L. Ivchenko, and U. Rössler, Phys. Rev. B **58**, 16353 (1998).
[22] S. J. Prado, C. Trallero-Giner, A. M. Alcalde, V. López-Richard, and G. E. Marques, Phys. Rev. B **69**, 201310(R) (2004).
[23] R. Kotlyar, T. L. Reinecke, M. Bayer, and A. Forchel, Phys. Rev. B **63**, 085310 (2001).
[24] S. Fafard and C. N. Allen, Appl. Phys. Lett. **75**, 2374 (1999).
[25] J. Tatebayashi, Y. Arakawa, N. Hatori, H. Ebe, M. Sugawara, H. Sudo, and A. Kuramata, Appl. Phys. Lett. **85**, 1024 (2004).
[26] W. Langbein, P. Borri, U. Woggon, V. Stavarache, D. Reuter, and A. D. Wieck Phys. Rev. B **69**, 161301(R) (2004).
[27] A. I. Tartakovskii, M. N. Makhonin, I. R. Sellers, J. Cahill, A. D. Andreev, D. M. Whittaker, J-P. R. Wells, A. M. Fox, D. J. Mowbray, M. S. Skolnick, K. M. Groom, M. J. Steer, H. Y. Liu, and M. Hopkinson, Phys. Rev. B **70**, 193303 (2004).
[28] W. Langbein, P. Borri, U. Woggon, V. Stavarache, D. Reuter, and A. D. Wieck, Phys. Rev. B **70**, 033301 (2004).
[29] B. Grandidier, Y. M. Niquet, B. Legrand, J. P. Nys, C. Priester, D. Stievenard, J. M. Gerard, and V. Thierry-Mieg, Phys. Rev. Lett. **85**, 1068 (2000).
[30] P. W. Fry, I. E. Itskevich, D. J. Mowbray, M. S. Skolnick, J. J. Finley, J. A. Barker, E. P. O'Reilly, L. R. Wilson, I. A. Larkin, P. A. Maksym, M. Hopkinson, M. Al-Khafaji, J. P. R. David, A. G. Cullis, G. Hill, and J. C. Clark, Phys. Rev. Lett. **84**, 733 (2000).
[31] S. Raymond, S. Studenikin, A. Sachrajda, Z. Wasilewski, S. J. Cheng, W. Sheng, P. Hawrylak, A. Babinski, M. Potemski, G. Ortner, and M. Bayer, Phys. Rev. Lett. **92**, 187402 (2004).
[32] K. Nishi, H. Saito, S. Suger, and J.-S. Lee, Appl. Phys. Lett. **74**, 1111 (1999).
[33] J. Tatebayashi, M. Nishioka, and Y. Arakawa, Appl. Phys. Lett. **78**, 3469 (2001).
[34] S. Kaiser, T. Mensing, L. Worschech, F. Klopf, J. P. Reithmaier, and A. Forchel, Appl. Phys. Lett. **81**, 4898 (2002).
[35] T. Ide, T. Baba, J. Tatebayashi, S. Iwamoto, T. Nakaoka, and Y. Arakawa, Appl. Phys. Lett. **85**, 1326 (2004).
[36] H. Y. Liu, I. R. Sellers, T. J. Badcock, D. J. Mowbray, M. S. Skolnick, K. M. Groom, M. Gutierrez, M. Hopkinson, J. S. Ng, J. P. R. David, and R. Beanland, Appl. Phys. Lett. **85**, 704 (2004).
[37] J. M. Luttinger, Phys. Rev. **102**, 1030 (1956).
[38] T. B. Bahder, Phys. Rev. B **41**, 11 992 (1990).
[39] C. K. Pidgeon and R. N. Brown, Phys. Rev. **146**, 575 (1966).
[40] O. Stier, M. Grundmann, and D. Bimberg, Phys. Rev. B **59**, 5688 (1999).
[41] C. Pryor, Phys. Rev. B **57**, 7190 (1998).
[42] W. Sheng and J.-P. Leburton, Phys. Rev. B **67**, 125308 (2003).
[43] S. Lee, O. L. Lazarenkova, P. von Allmen, F. Oyafuso, and G. Klimeck, Phys. Rev. B **70**, 125307 (2004).
[44] T. Nakaoka, T. Saito, J. Tatebayashi, and Y. Arakawa, Phys. Rev. B **70**, 235337 (2004).
[45] T. Nakaoka, S. Kako, S. Ishida, M. Nishioka, and Y. Arakawa, Appl. Phys. Lett. **81**, 3954 (2002).
[46] J. Shumway, A. J. Williamson, A. Zunger, A. Passaseo, M. DeGiorgi, R. Cingolani, M. Catalano, and P. Crozier, Phys. Rev. B **64**, 125302 (2001), and references therein.
[47] P. A. Crozier, M. Catalano, R. Cingolani, and A. Passaseo, Appl. Phys. Lett. **79**, 3170 (2001).
[48] The reduction of $|g_{ex}|$ is hardly explained by dot size variations. As shown in Ref. 44, reduction of $|g_{ex}|$ can be caused by an increase of quantum confinement which seems unlikely to be accompanied by thermal annealing or intermixing. In addition, small dot size variations following the annealing are supported by similar diamagnetic shifts between annealed dots and as-grown ones.
[49] K. Takemoto, Y. Sakuma, S. Hirose, T. Usuki, N. Yokoyama, T. Miyazawa, M. Takatsu, and Y. Arakawa, Jpn. J. Appl. Phys., Part 2 **43**, L993 (2004).